Journal of Materials Chemistry A

PAPER

View Article Online
View Journal | View Issue

Cite this: J. Mater. Chem. A, 2015, 3, 22663

A self-powered system based on triboelectric nanogenerators and supercapacitors for metal corrosion prevention†

Xiaoyi Li,‡[abc] Juan Tao,‡[b] Wenxi Guo,[bd] Xiaojia Zhang,[b] Jianjun Luo,[b] Mengxiao Chen,[b] Jing Zhu*[ac] and Caofeng Pan*[b]

Received 5th September 2015
Accepted 4th October 2015

DOI: 10.1039/c5ta07053h

www.rsc.org/MaterialsA

As water covers most of the earth's surface, the energy of the ocean is abundant and almost unexplored, which can be one of the most environmentally friendly forms of energy. Prevention of metal corrosion plays an important role in national economic development and daily life. Here, we report a network of triboelectric nanogenerators (TENGs) and supercapacitors (SCs), which is also called the self-powered system, to harvest a huge amount of water energy for preventing metal corrosion. When the TENG is integrated with a SC, the output current is stable and continuous. The corrosion results indicate that the TENG-SC self-powered system can prevent about 80% degree of corrosion for Q235 steel in 0.5 M NaCl solution. This work demonstrates that the TENG-SC system, which is self-powered, flexible and environmentally friendly, can harvest and store large-scale blue energy from the ocean, and also renders an innovative approach toward preventing the metal corrosion without other power sources.

1. Introduction

Corrosion protection of metals plays an important role in national economic development and daily life.[1,2] So far, tremendous efforts have been devoted to protecting the metals from corrosion and cathodic protection is considered as one of the most effective ways.[3,4] However, the traditional cathodic protection needs either a sacrificial anode or an external power source, which increases costs and limits its applications.[5] Therefore, constructing an integrated system which can easily harvest and store the renewable energy from the environment will render an innovative and effective approach to prevent metal corrosion.

As water widely distributes across the earth's surface, the energy of the ocean is abundant, clean and renewable, which contributes to the sustainable development of human civilization. The blue energy from the ocean, which is less dependent on season, circadian rhythm, weather or temperature, has several advantages compared with other renewable energies. Although numerous research studies have been committed to harvesting the massive blue energy, the utilization of water wave energy needs to be further developed. Furthermore, corrosion is more likely to take place in metals under the ocean environmental conditions. Triboelectric nanogenerators (TENGs), which convert the mechanical energy to electricity, can solve the problem.[6–9]

Here, we report a network of triboelectric nanogenerators (TENGs) and supercapacitors (SCs), also called the self-powered system, to harvest a huge amount of water energy for preventing metal corrosion. The short-circuit current and open-circuit voltage of the TENGs are 5 μA and 75 V. When integrated with SCs, the output current of the device is stable and continuous. The corrosion results illustrate that the TENG-SC self-powered system can prevent about 80% degree of corrosion for Q235 steel in 0.5 M NaCl solution. This technology provides an innovative and effective way to collect a huge amount of blue energy from the ocean and renders an original and effective approach to prevent metal corrosion without other power sources. The concepts and studies in this article can be used in a variety of applications and improve our living.

2. Experimental section

2.1 Fabrication and measurement of TENGs

A 30 μm-thick polytetrafluoroethylene (PTFE) film was adopted to be the friction material. After cleaning with alcohol and deionized water (DIW), the PTFE film was coated with a 10 nm thick Au film by magnetron sputtering (Discovery 635, Denton

[a]National Center for Electron Microscopy in Beijing, School of Materials Science and Engineering, The State Key Laboratory of New Ceramics and Fine Processing, Key Laboratory of Advanced Materials (MOE), Tsinghua University, Beijing, China. E-mail: jzhu@mail.tsinghua.edu.cn

[b]Beijing Institute of Nanoenergy and Nanosystems, Chinese Academy of Sciences, Beijing, China. E-mail: cfpan@binn.cas.cn

[c]Center for Nano and Micro Mechanics, Tsinghua University, Beijing 100084, China

[d]Research Institution for Biomimetics and Soft Matter and Department of Physics, Xiamen University, Xiamen, 361005, PR China

† Electronic supplementary information (ESI) available: Fig. S1–4. See DOI: 10.1039/c5ta07053h

‡ Authors contributed equally to this work.

Vacuum). Then the film was etched by inductively coupled plasma (ICP) to create PTFE nanowires on the surface. Two copper electrodes (12 cm × 2 cm) were deposited onto the back of the PTFE film by magnetic sputtering at 60 w for 30 min. Finally, the PTFE film with two copper electrodes was attached to a flexible acrylic substrate with the electrodes inside. And a pump (Jebao ECO) was used to generate water waves by controlling the movement of water to simulate the marine environment. The short-circuit current was measured by using an SR570 (Stanford Research System), and induced charge and open-circuit voltage were both tested by using a Keithley 6514 electrometer.

2.2 Preparation of SCs

The highly flexible and transparent network electrodes for SCs were produced using the electrospinning and sputtering method which was suggested by previous studies.[10,11] First of all, 8 wt% polyvinyl butyral (PVB) alcohol solution was prepared at room temperature, and the PVB fibers were obtained by electrostatic spinning (TJ-8JNY) at the positive voltage 17 kV. Then, the PVB fibers were coated with a thin silver layer by magnetic sputtering at 100 w for 10 min and the core–shell fibers were immersed in DIW to dissolve the PVB. The Ag networks were then transferred to a polyethylene terephthalate (PET) substrate. The gel electrolyte of SCs was obtained by continuously adding PVA powder (25 g) and phosphoric acid (H_3PO_4, 20 g) into DIW (250 ml) at 90 °C with stirring. Subsequently, the PVA/H_3PO_4 gel electrolyte was spin-coated on the PET/Ag network electrode at 1000 r min^{-1} for 1 min. Finally, the cellulose acetate membrane was utilized as a separator.[12] Symmetrical electrodes were adopted to construct the SCs in this study. The cyclic voltammetry (CV) curves were measured by using an SR570 with D345 and the galvanostatic charge/discharge (GCD) curves were tested by using a Cell Testing System (LANHE). An autolab electrochemical workstation (Autolab, Eco-Chemie) was used to measure the open circuit potential.

3. Results and discussion

As reported in our previous study, it has been demonstrated that water can provide the power which can generate triboelectricity, and that the contact electrification between water and insulating polymer films has been used to harvest wave energy.[13–19] Fig. 1 shows a schematic diagram and the output signals of the flexible TENG. Fig. 1a illustrates the working principle of the TENG which harvests the mechanical energy of water and converts it to electricity. When the PTFE thin film with two Cu electrodes at the backside is immersed into water, surface triboelectric charges arise at the water–PTFE interface. And because of the asymmetric surface charges, free electrons are induced to flow between the two electrodes during the emerging and submerging processes. The working mechanism of the TENG is shown in Fig. S1.† In order to enhance the output of the TENG, the PTFE surface is etched to create the nanowire arrays to increase the effective contact area. The SEM image of

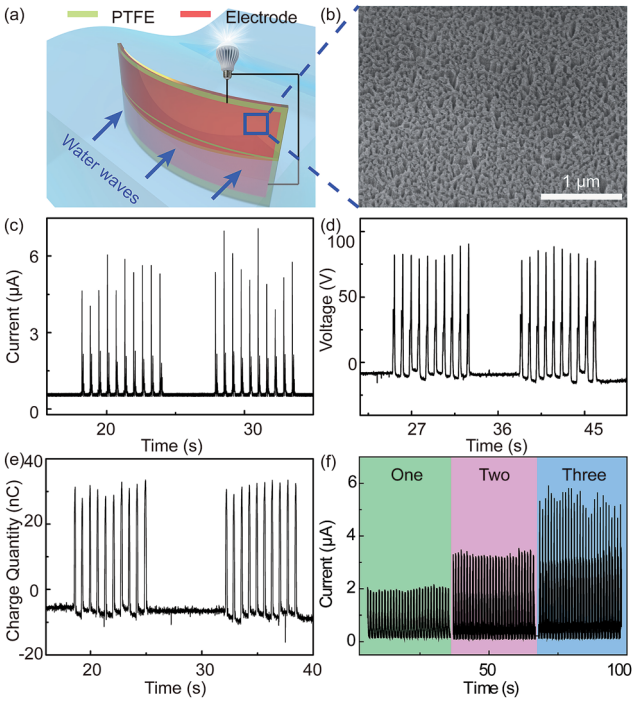

Fig. 1 (a) Schematic diagram of the bent TENG in water waves. The up/down movement of the water surrounding the TENG induces electricity produced between the two electrodes. (b) SEM image of the polymer (PTFE) nanowires on the top surface of the polymer layer (PTFE). The short-circuit current (c), open-circuit voltage (d) and induced charges (e) of the TENG with the up and down movement in water. (f) The rectified short-circuit current of TENGs with the unit number n = 1, 2, 3.

the PTFE nanowire arrays is presented in Fig. 1b. It can be found that the PTFE nanowires are uniformly distributed on the surface with an average diameter of 50 nm. According to the previous work reported by Zhu *et al.*, because of their uniform super hydrophobic properties and considerable surface areas, these nanowires play an important role in the process of harvesting water mechanical energy. In order to evaluate the electrical output performance of the TENG (100 mm × 42 mm, shown in Fig. S2b†) with water, the short-circuit current (Fig. 1c), open-circuit voltage (Fig. 1d) and charge quantity (Fig. 1e) are measured when the TENG moves up and down in water. The peak of the current shown in Fig. 1c is about 5 μA and the open-circuit voltage shown in Fig. 1d can reach about 75 V. And the total amount of induced charges is about 30 nC as shown in Fig. 1e in one emerging and submerging process. The electrical signals (including current, voltage and induced charges) increase when increasing the speed of the wave.[11] To develop a TENG network, thousands of TENGs are electrically connected in parallel to develop a network. And a pump is utilized to generate water waves by controlling the movement of water to simulate the marine environment. To reveal the mechanism of the TENG networks for blue energy harvesting, three TENGs are fabricated into a small network (Fig. S2a†). Fig. 1f demonstrates the output current of the small TENG network with the unit number n = 1, 2, 3, respectively. It is

obvious that the current output increases when the unit number increases from 1 to 3.

Because the output signals of the TENG are pulsed and non-continuous, a flexible supercapacitor is designed to store the energy from the TENG and convert it to a more stable and continuous form. Fig. 2a shows the schematic image of the flexible electrical double-layer supercapacitor with Ag network electrodes on a PET substrate. The device consists of four components: the PET substrate, the Ag network electrodes, the solid electrolytes and a separator. The optical images of a typical SC in Fig. 2b and c show that the SC is diaphanous and flexible with great potential in energy storage, flexible device and transparent electronic device applications.[20] The PVB networks shown in Fig. 2d are fabricated by electrostatic spinning. After depositing Ag on the surface of the PVB fibers as shown in Fig. 2e, the obtained core–shell networks are immersed in DIW to remove the PVB. It can be observed that PVB networks are uniformly intertwined, which enables network electrodes to present good conductivity after depositing metal Ag. The average diameter of the Ag fibers is about 3 μm and the convex surface is rough with nano-structures (Fig. S3†), therefore the surface area of the electrodes can be remarkably enhanced. The micro- and nano-structures of materials increase the contact surface area between the electrode and the electrolyte.[21,22] The cyclic voltammetry (CV) curves of the flexible device with the scan rate ranging from 20 to 1000 mV s^{-1} are performed in the potential window of 0 to 0.8 V, as shown in Fig. 2e. These CV curves are found to be rectangular in shape within a selected range of potential even at high scan rates, indicating the fast diffusion of ions and a very rapid current response to voltage reversal in the active materials of electrodes. The CV curves in the potential windows of 0 to 0.6 V, 0 to 0.8 V and 0 to 1 V with the same scan rate 500 mV s^{-1} are shown in Fig. 2f. The CV curves exhibit similar rectangle-like shapes even at a wide potential window, which indicates good rate capability, ideal supercapacitor behaviour and excellent stability of electrodes.[23,24]

Fig. 3a shows the GCD curves of the supercapacitor at the different current values ranging from 5 to 50 μA. The GCD curves are similar in shape between 0 and 0.8 V and are nearly triangular in shape during the charge–discharge cycles, which indicates that the supercapacitor can stably perform in various current values and also exhibit good symmetry.[25] The almost linear slopes at high discharge current values illustrate the electrochemical double layer behavior and further confirm the capacitive and fast charge/discharge properties of the supercapacitor.[21,26,27] According to GCD tests, the supercapacitor exhibits the highest capacitance of 1128 μF at a discharge current of 5 μA as shown in Fig. 3b. It can be seen that the capacitance decreases gradually and tends to be stable eventually with an increase in the current value from 5 to 50 μA, which can be attributed to progressively less efficient infiltration of ions into electrodes at higher scan rates.[28–30] At the lower current scan rates, the ions have sufficient time to gain access to diffuse from the electrolyte deep into electrodes. Nevertheless, there is no enough time for the ions to diffuse with the enhancement of scan rates, which causes the reduction of capacitance. The Ag network electrode with excellent electrical conductivity and

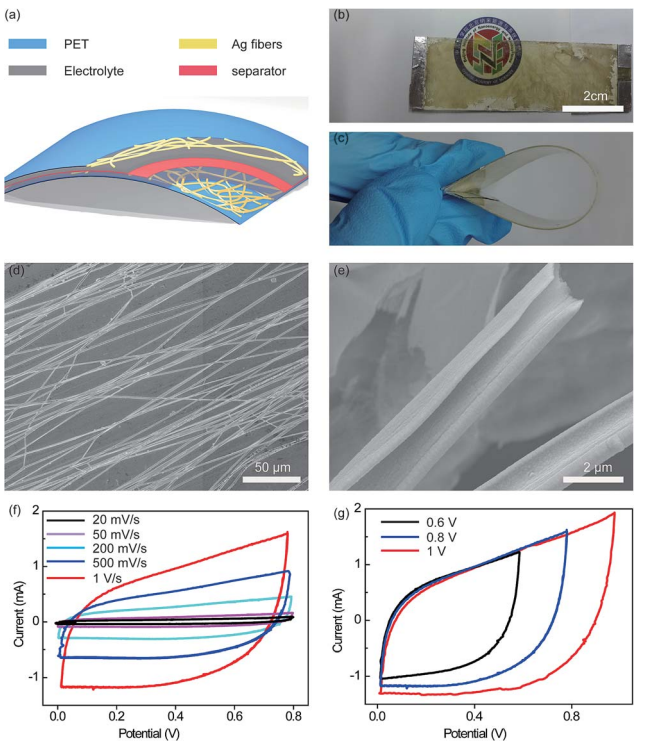

Fig. 2 (a) Schematic of the flexible electrical double-layer supercapacitor (SC). Optical images of the diaphanous supercapacitor (b) and the flexible supercapacitor (c). SEM images of PVB fibers (d) and Ag fibers (e) by depositing Ag on the surface of PVB fibers and dissolving the PVB. (f) CV curves of the diaphanous flexible supercapacitor at different scan rates (20–1000 mV s^{-1}). (g) CV curves of the supercapacitor measured at different voltage windows.

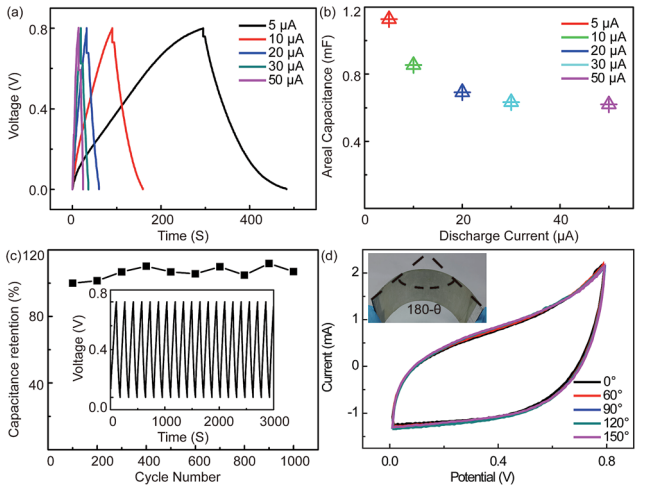

Fig. 3 (a) Galvanostatic charge–discharge curves of the SC at the different current values ranging from 5 to 50 μA. (b) The capacitance under different discharge currents. (c) Variation of capacitance stability of the SC with the cycle number at the current of 50 μA. The inset picture is the charge–discharge curves of the SC at 10 μA by 30 circles. (d) CV of the SC before bending ($\theta = 0°$) and while being bent ($\theta = 60°$, 90°, 120° and 150°).

a high surface area can guarantee excellent capacitive behavior. The cycle stability is an important parameter of a SC for its practical applications. Fig. 3c shows the long-term stability of the SC for 1000 cycles at a current of 50 μA. Interestingly, it can be observed that the discharge capacitance of the SC slightly increases and remains stable after 300 cycles. The electrolyte gradually penetrates into the hollow structure of the Ag network with the increase of the effective interfacial area between the electrode and electrolyte, which causes the increase in capacitance.[12] The inset in Fig. 3c shows typical charge–discharge curves in a continuous operation for 30 cycles. In order to study the flexibility of the supercapacitor, the CV curves of the supercapacitor before and while being bent are performed under different bending angles. And no significant deviation of the CV curves is observed when the device is bent even to 150° as shown in Fig. 3d and 2b, indicating that it possesses an excellent flexibility. The remarkable cycling stability, mechanical flexibility and capacitance retention of the flexible SC devices will be beneficial for their practical applications.

To develop a TENG-SC network, thousands of TENG-SCs are electrically connected in parallel to develop a network for blue energy harvesting, as shown in Fig. 4a. Fig. 4b demonstrates the charge quantity of the SC powered by a TENG. When the TENG is turned on, a large quantity of charges are injected into the SC causing a rapid rise while the charge quantity stays stable when the TENG is off. In Fig. 4c, the current of the SC charged by the TENG is the left part and discharging current of the SC with the external resistance of 100 kΩ is the right part. Since the output signals of the TENG are pulsed, the current flowing into the SC is also non-continuous as shown in the inset of Fig. 4c. But when the SC discharges with an external resistance of 100 kΩ, the output current is a direct current and continuous, which is significant for its potential applications. The circuit diagram is shown in Fig. S2c.† This technology provides an innovative and effective method to collect a huge amount of blue energy from the ocean. And the energy stored in the SCs can be used for metal corrosion prevention,[8] replacing the batteries or powering the ocean environment monitoring sensors.

The energy generated from the TENG and stored in the SC can be used in a variety of applications and improve our living. Fig. 5a shows the structure and working principle of the TENG-SC cathodic protection system. When the TENGs start to harvest the mechanical energy of the water wave (0.2 m s^{-1}, 1 Hz), the transferred electrons will be injected into the protected steels, resulting in a cathodic polarization. Fig. 5b indicates the open circuit potential of the 403SS steel electrode immersed in 0.5 M NaCl solution. When the TENG-SC system is not working, the potential of the steel electrode is about −0.35 V. It exhibits a drastic negative shift to −0.6 V when the TENG is turned on, shown as the green part in Fig. 5b, indicating that the steel become more stable with the help of the SC. It is worth noting that when the TENG is turned off, the potential will not recover to its original value quickly but stays at another platform at about −0.5 V for a while, as shown in the purple part of Fig. 5b.

Finally, the weight-loss tests for Q235 carbon steels are also carried out to further evaluate the corrosion protection capacity

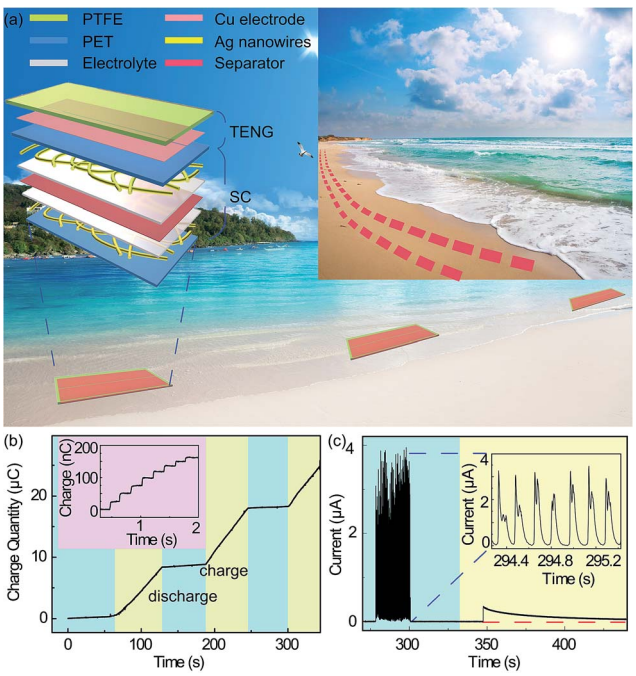

Fig. 4 (a) Schematic illustration of the power pack (TENGs and SCs) networks which consist of thousands of single units on the beach. The power pack networks are built on the beach to harvest the wave energy and store the electric energy. (b)The charge quantity of the supercapacitor charged by using the TENG. (c) The current of the SC charged by using the TENG and the discharging current of the SC with the external resistance of 100 kΩ. The SC converts the pulsed current generated by the TENG to a stable and continuous signal.

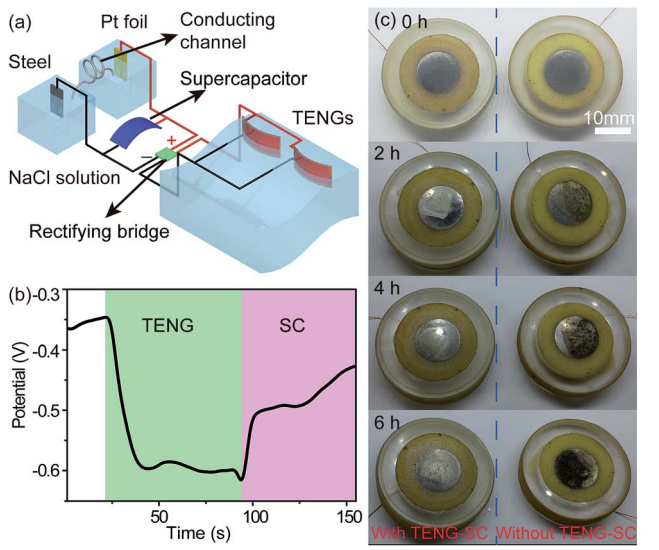

Fig. 5 (a) The structure and working principle of the TENG-SC cathodic protection system. (b) The open circuit potential changes of a pure 403SS electrode coupled with and without the power pack. (c) The digital photographs of the surface morphology of Q235 carbon steels after immersing in 0.5 M NaCl solution for different times. The Q235 specimens are separated into two groups; one group specimens (on the left) are coupled to the negative pole of three power packs while the others (on the right) are not.

of our TENG-SC cathodic protection system. The optical images of the surface morphology of the Q235 carbon steels with and without the TENG-SC self-powered system for different times are shown in Fig. 5c. It is obvious that the steel without TENG-SC has much more red rust on the surface than that with TENG-SC after 1–2 h of immersion. Generally once the corrosion spots appear on the surface of the steel, the corrosion rate increases quickly and a large quantity of rust expands on the surface. After 6 h of immersion in the 0.5 M NaCl solution, a thick film of rust covers the surface of steel without TENG-SC, while still only a few corrosion spots remain on the steel with TENG-SC. The results greatly prove that the TENG-SC self-powered system can effectively reduce the corrosion rate. Furthermore, SEM images of the steels with and without TENG-SC are shown in Fig. S4,† which also indicates that the TENG-SC self-powered system can prevent metal corrosion significantly. It has been proved in our previous work that the open circuit potential of the steel decreases when the external solution resistance increases.[8] The weight-loss tests demonstrate that the TENG-SC self-powered system can prevent about 80% degree of corrosion for Q235 steel in 0.5 M NaCl solution when the external resistance is 0.2 MΩ.

4. Conclusions

We report a network of TENGs and SCs, which is also called the self-powered system, to harvest a huge amount of water energy for preventing metal corrosion. The TENG delivers a short-circuit current of 5 μA and an open-circuit voltage of 75 V. When integrated with a SC, the output current of the device is stable and continuous. The corrosion results illustrate that the TENG-SC self-powered system can prevent about 80% degree of corrosion for Q235 steel in 0.5 M NaCl solution. With the high sensitivity to water waves, the TENG-SC self-powered system can not only be used in strong wave circumstances (ocean) but also applied in many other conditions, such as lake, river and swimming pool. This technology provides a self-powered, flexible, extremely cost-effective, lightweight, environmentally friendly and easily implemented system to harvest a huge amount of blue energy from the ocean. In addition, our TENG-SC can be integrated with solar cells or wind energy collectors to harvest various kinds of energies,[31] which can be immediately adopted in a variety of applications, such as preventing metal corrosion,[32] replacing batteries and powering ocean environment monitoring sensors.

Acknowledgements

This work was financially supported by the "thousands talents" program for pioneer researcher and his innovation team, China; National 973 Project of China (2015CB654902); Chinese National Natural Science Foundation (11374174, 51390471); President Funding of the Chinese Academy of Sciences; National Natural Science Foundation of China (No. 51272238, 21321062, 51432005 and 61405040); Beijing City Committee of science and technology (Z131100006013004, Z131100006013005). This work made use of the resources of the National Center for Electron Microscopy in Beijing and Beijing Institute of Nanoenergy and Nanosystems, Chinese Academy of Sciences.

Notes and references

1 C. Punckt, M. Bolscher, H. H. Rotermund, A. S. Mikhailov, L. Organ, N. Budiansky, J. R. Scully and J. L. Hudson, *Science*, 2004, **305**, 1133–1136.
2 H. Park, K. Y. Kim and W. Choi, *Chem. Commun.*, 2001, 281–282.
3 M. M. S. Cheung and C. Cao, *Constr. Build. Mater.*, 2013, **45**, 199–207.
4 J. Xu and W. Yao, *Constr. Build. Mater.*, 2009, **23**, 2220–2226.
5 S. Yehia and J. Host, *ACI Mater. J.*, 2010, **107**, 577–585.
6 C. F. Pan, Z. T. Li, W. X. Guo, J. Zhu and Z. L. Wang, *Angew. Chem., Int. Ed.*, 2011, **50**, 11192–11196.
7 S. Wang, L. Lin and Z. L. Wang, *Nano Lett.*, 2012, **12**, 6339–6346.
8 W. X. Guo, X. Y. Li, M. X. Chen, L. Xu, L. Dong, X. Cao, W. Tang, J. Zhu, C. J. Lin, C. F. Pan and Z. L. Wang, *Adv. Funct. Mater.*, 2014, **24**, 6691–6699.
9 S. Wang, L. Lin, Y. Xie, Q. Jing, S. Niu and Z. L. Wang, *Nano Lett.*, 2013, **13**, 2226–2233.
10 H. Wu, D. S. Kong, Z. C. Ruan, P. C. Hsu, S. Wang, Z. F. Yu, T. J. Carney, L. B. Hu, S. H. Fan and Y. Cui, *Nat. Nanotechnol.*, 2013, **8**, 421–425.
11 W. X. Guo, X. J. Zhang, R. M. Yu, M. L. Que, Z. M. Zhang, Z. W. Wang, Q. L. Hua, C. F. Wang, Z. L. Wang and C. F. Pan, *Adv. Energy Mater.*, 2015, **5**, 1500141.
12 S. H. Li, D. K. Huang, B. Y. Zhang, X. B. Xu, M. K. Wang, G. Yang and Y. Shen, *Adv. Energy Mater.*, 2014, **4**, 1301655.
13 G. Zhu, Y. J. Su, P. Bai, J. Chen, Q. S. Jing, W. Q. Yang and Z. L. Wang, *ACS Nano*, 2014, **8**, 6031–6037.
14 Z. H. Lin, G. Cheng, S. Lee, K. C. Pradel and Z. L. Wang, *Adv. Mater.*, 2014, **26**, 4690–4696.
15 Z. H. Lin, G. Cheng, L. Lin, S. Lee and Z. L. Wang, *Angew. Chem., Int. Ed.*, 2013, **52**, 12545–12549.
16 Z. H. Lin, G. Cheng, W. Z. Wu, K. C. Pradel and Z. L. Wang, *ACS Nano*, 2014, **8**, 6440–6448.
17 M. X. Chen, X. Y. Li, L. Lin, W. M. Du, X. Han, J. Zhu, C. F. Pan and Z. L. Wang, *Adv. Funct. Mater.*, 2014, **24**, 5059–5066.
18 J. Chen, J. Yang, Z. L. Li, X. Fan, Y. L. Zi, Q. S. Jing, H. Y. Guo, Z. Wen, K. C. Pradel, S. M. Niu and Z. L. Wang, *ACS Nano*, 2015, **9**, 3324–3331.
19 G. Cheng, Z. H. Lin, Z. L. Du and Z. L. Wang, *ACS Nano*, 2014, **8**, 1932–1939.
20 Y. Hou, L. Y. Chen, P. Liu, J. L. Kang, T. Fujita and M. W. Chen, *J. Mater. Chem. A*, 2014, **2**, 10910–10916.
21 X. L. Chen, H. J. Lin, J. Deng, Y. Zhang, X. M. Sun, P. N. Chen, X. Fang, Z. T. Zhang, G. Z. Guan and H. S. Peng, *Adv. Mater.*, 2014, **26**, 8126–8132.
22 B. Y. Ahn, E. B. Duoss, M. J. Motala, X. Y. Guo, S. I. Park, Y. J. Xiong, J. Yoon, R. G. Nuzzo, J. A. Rogers and J. A. Lewis, *Science*, 2009, **323**, 1590–1593.
23 K. Y. Xie and B. Q. Wei, *Adv. Mater.*, 2014, **26**, 3592–3617.

24 X. F. Wang, X. H. Lu, B. Liu, D. Chen, Y. X. Tong and G. Z. Shen, *Adv. Mater.*, 2014, **26**, 4763–4782.
25 L. B. Hu, H. Wu, F. La Mantia, Y. A. Yang and Y. Cui, *ACS Nano*, 2010, **4**, 5843–5848.
26 Z. Zheng, J. J. Chen, R. Yoshida, X. Gao, K. Tarr, Y. H. Ikuhara and W. L. Zhou, *Nanotechnology*, 2014, **25**, 435406.
27 Z. Niu, L. Zhang, L. Liu, B. Zhu, H. Dong and X. Chen, *Adv. Mater.*, 2013, **25**, 4035–4042.
28 S. J. He and W. Chen, *Nanoscale*, 2015, **7**, 6957–6990.
29 Z. J. Su, C. Yang, B. H. Xie, Z. Y. Lin, Z. X. Zhang, J. P. Liu, B. H. Li, F. Y. Kang and C. P. Wong, *Energy Environ. Sci.*, 2014, **7**, 2652–2659.
30 F. Zhang, T. F. Zhang, X. Yang, L. Zhang, K. Leng, Y. Huang and Y. S. Chen, *Energy Environ. Sci.*, 2013, **6**, 1623–1632.
31 X. B. Xu, S. H. Li, H. Zhang, Y. Shen, S. M. Zakeeruddin, M. Graetzel, Y. B. Cheng and M. K. Wang, *ACS Nano*, 2015, **9**, 1782–1787.
32 X. J. Zhao, G. Zhu, Y. J. Fan, H. Y. Li and Z. L. Wang, *ACS Nano*, 2015, **9**, 7671–7677.